Monserrat López, A.; Miguel Sosa, P.; Bonet Senach, JL.; Fernández Prada, MÁ. (2020). Influence of the plastic hinge rotations on shear strength in continuous reinforced concrete beams with shear reinforcement. Engineering Structures. 207:1-14. https://doi.org/10.1016/j.engstruct.2020.110242

INFLUENCE OF THE PLASTIC HINGE ROTATIONS ON SHEAR STRENGTH IN CONTINUOUS REINFORCED CONCRETE BEAMS WITH SHEAR REINFORCEMENT

Andrea Monserrat López, anmonlo6@upv.es

Pedro Fco. Miguel Sosa, pmiguel@cst.upv.es

José Luis Bonet Senach, jlbonet@cst.upv.es

Miguel Ángel Fernández Prada, mafernan@cst.upv.es

Universitat Politècnica de València, Camí de Vera s/n, 46022, Valencia, Spain

Abstract

Continuous reinforced concrete (RC) beams may develop significant plastic rotations to enable the redistribution of bending moments. These rotations occur at plastic hinges, which are subject to high shear forces. The influence of rotations on the shear strength for members without shear reinforcement failing in shear after yielding of the flexural reinforcement has already been experimentally verified in continuous RC beams. However, this influence has not been studied in continuous members with shear reinforcement. An innovative tests system has been specially designed to develop shear failures before and after yielding of the flexural reinforcement in both statically determinate and indeterminate structures.

Nine beams (9,000 mm long, 250 mm wide, 450 mm high) with a shear reinforcement of ϕ8/30 (ρ_w = 0.13%) and different longitudinal reinforcement ratios were tested under different load and support conditions.

The shear strength provided by shear reinforcement and that provided by the other mechanisms of resistance (shear strength provided by concrete) for each specimen were calculated based on the critical shear crack width measurements taken by Digital Image

Correlation (DIC). Bending rotation and crack rotation along the development length of the critical shear crack were also obtained by DIC.

Based on the test results, the shear strength provided by concrete was studied in relation to the bending rotation and the average crack width in reinforced concrete beams with shear reinforcement. It was confirmed that the shear strength provided by concrete decreased with increasing both bending rotations and crack widths. The shear strength values predicted by different design codes (ACI 318-19, Eurocode 2 and Model Code 2010) were compared with the test results, and showed that these formulations did not properly capture the loss of shear strength caused by bending rotations.

Keywords

Shear test, shear strength, reinforced concrete, continuous beam, shear reinforcement, plastic hinge.

Highlights

Development of an innovative tests system with statically indeterminate structures

Digital Image Correlation techniques used to measure bending rotation

Crack rotation detected by a different rotation of bodies over and below the CSC

Shear strength provided by concrete decreases with bending rotation and crack width

Codes do not properly capture the shear strength reduction due to bending rotation

Abbreviations

A_s	area of tension reinforcement
A'_s	area of compression reinforcement
a	shear span (defined as M/V)
b	concrete section width
c	concrete cover
d	effective depth
E_c	modulus of elasticity of concrete
E_s	modulus of elasticity of reinforcement
f_c	compressive strength of concrete measured in cylinder
f_{ct}	tensile strength of concrete
f_u	tensile strength of reinforcement
$f_{u,sw}$	tensile strength of a single stirrup
f_y	yield strength of reinforcement
$f_{y,sw}$	yield strength of a single stirrup
l_i	length of cantilever (i = 1,3) or span (i = 2)
l_j	distance between crack *i* and the DIC measurement *j* point
l_k	distance between crack *i* and the DIC measurement *k* point
l_x	segment of the span (x = a,b,c)
M_1	bending moment (section of support A in CE, section of support B in SE)
M_2	bending moment (section of applied load P_2 in SE)
$M_{1,R}$	bending moment at failure (section of support A in CE, section of support B in SE)
$M_{2,R}$	bending moment at failure (section of applied load P_2 in SE)
M_{pl}	bending moment at the yielding of flexural reinforcement
P_i	applied load (i = 1,2)
$P_{i,R}$	applied load (i = 1,2) at failure
R_A	reaction in support section A
R_B	reaction in support section B
V	shear force
V_c	shear strength provided by concrete
$V_{c,test}$	shear strength provided by concrete in tests
$V_{R,test}$	shear strength in tests
V_{Rd}	predicted shear strength by design code
V_s	shear strength provided by shear reinforcement
V_{sw}	shear force provided by a single stirrup
$V_{s,test}$	shear strength provided by shear reinforcement in tests
w_i	crack width of crack *i*
w_{st}	average value of the critical shear crack opening measured in the stirrups section
γ_c	partial safety factor for concrete material properties

1	$\boldsymbol{\delta_b}$	relative concrete-steel slip
2	$\boldsymbol{\delta_{by}}$	relative concrete-steel slip at yielding
3	$\boldsymbol{\delta_i}$	beam deflection under applied load (i = 1,2)
4	$\boldsymbol{\delta_s}$	vertical displacement due to shear deformation
5	ε_{sw}	strain of a single stirrup
6	$\varepsilon_{s,2d}$	top flexural reinforcement middle strain along 2d length
7	$\boldsymbol{\varepsilon_u}$	reinforcement strain at maximum load
8	$\boldsymbol{\varepsilon_{u,sw}}$	strain at maximum load of a single stirrup
9	$\boldsymbol{\varepsilon_y}$	yield strain of reinforcement
10	$\boldsymbol{\varepsilon_{y,sw}}$	yield strain of a single stirrup
11	$\boldsymbol{\theta}$	angle between web compression and the axis of the member
12	$\boldsymbol{\theta_B}$	slope at the support $\boldsymbol{B}$ in the SE tests
13	$\boldsymbol{\theta_{B,I}}$	slope at the support $\boldsymbol{B}$ at the end of the first phase in the SE tests
14	$\boldsymbol{\rho}$	reinforcement ratio of tension reinforcement
15	$\boldsymbol{\rho_w}$	reinforcement ratio of shear reinforcement
16	$\boldsymbol{\sigma_{sw}}$	stress for a single stirrup
17	$\boldsymbol{\tau_b}$	bond stress of reinforcement
18	$\boldsymbol{\tau_{b1}}$	bond stress prior to yielding of reinforcement
19	$\boldsymbol{\tau_{b2}}$	bond stress after yielding of reinforcement
20	$\boldsymbol{\phi}$	nominal diameter of a reinforcing bar
21	ψ	rotation of beams
22	$\boldsymbol{\psi_b}$	bending rotation of beams
23	$\boldsymbol{\psi_{pl}}$	rotation of beams at yielding of the flexural reinforcement
24	$\boldsymbol{\psi_s}$	crack rotation
25	$\boldsymbol{\psi_t}$	total rotation of beams

1. Introduction

Statically indeterminate reinforced concrete structures, such as bridges or building frames, may develop significant plastic rotations to enable the redistribution of bending moments before developing their full structural strength. The regions where plastic rotations take place (plastic hinges) are usually subject to high shear forces, which may reduce the rotation capacity if a shear failure occurs after yielding of the flexural reinforcement. The interaction may be considered as a reduction of the shear strength because of the flexural deformation developed in the critical plastic regions. This interaction may be particularly relevant on statically indeterminate structures, which may fail in shear after yielding of the flexural reinforcement and with increasing shear forces at the critical plastic regions.

In statically determinate structures, members can fail in shear before yielding of the flexural reinforcement (branch A, **Fig. 1**) or afterwards (branch B, **Fig. 1**). In the latter case, shear forces cannot increase after yielding as the flexural capacity of the structure has already been attained.

However, the structural behaviour of a statically indeterminate structure enables shear failures after yielding of the flexural reinforcement to be developed with increasing shear forces as its flexural capacity is not attained until all the possible plastic hinges along the structure have been developed. So, members can fail in shear after yielding of the flexural reinforcement while shear forces increase (branch C, **Fig. 1**) or with a constant shear force after all the plastic hinges have been developed; that is, when the full structural strength has been attained (branch D, **Fig. 1**). In any case, in a statically indeterminate structure such as a continuous beam, the large deformation levels that may be reached in the critical plastic zones where large shear forces are acting may cause a loss of shear strength.

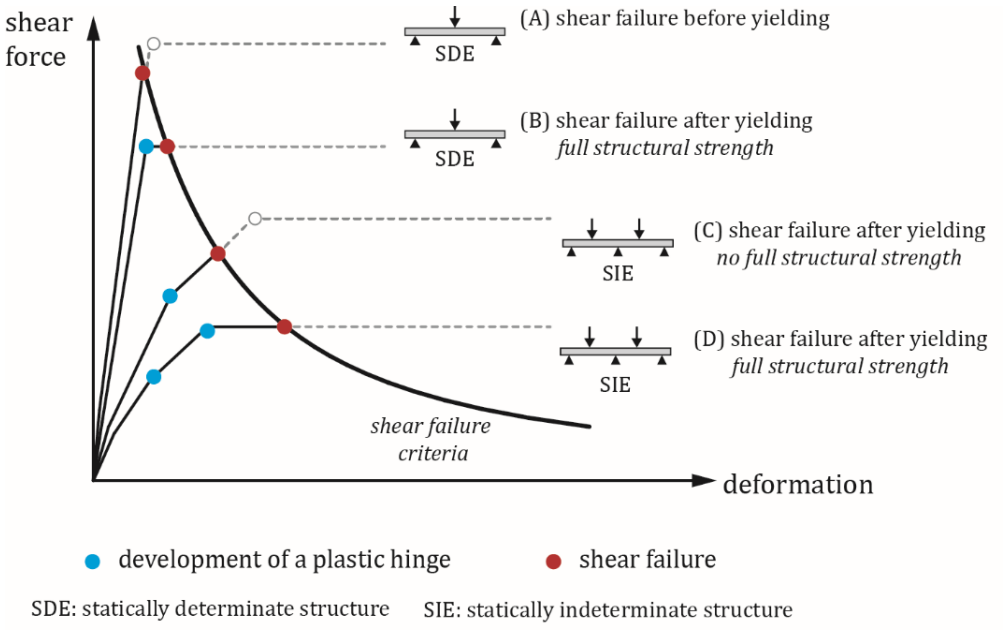

Fig. 1. Behaviour of structural determinate and indeterminate structures failing in shear before and after yielding of the flexural reinforcement.

The interaction between rotations and shear forces in critical zones of reinforced concrete members has been studied in statically determinate structures. Lopes and do Carmo [1] presented a theoretical model to evaluate the plastic rotation capacity of a critical zone subject to shear force. Vaz Rodriges et al. [2] experimentally studied the influence of shear on the rotation capacity of 11 slab strips without shear reinforcement. They concluded that the rotation capacity of plastic hinges increases for lowering shear force values.

The most relevant shear design formulations for members with shear reinforcement have different ways of considering the deformation of critical zones. For example, strut-and-tie models [3] (started with truss analogy [4,5]) and stress fields [6] (a direct approach of the theory of plasticity) are based on equilibrium considerations. However, the modified compression field theory (MCFT) [7,8] considers equilibrium and compatibility conditions and the softening compressive strength of cracked concrete.

The first studies conducted by Leonhardt [9,10] showed the influence of concrete on shear strength, and later physical models and constitutive laws indicated normal and

tangential stresses transferred along crack surfaces due to aggregate interlocking [11–15]. Later, the crack friction, as a transfer action for resisting shear force, was considered to modify the truss model [16–18].

Recently, different approaches considering a combination of several shear transfer mechanisms to explain shear strength have been investigated. On the one hand, the influence of the deformation of a member on its shear strength for reinforced concrete (RC) members without shear reinforcement has been studied and demonstrated by the critical shear crack theory (CSCT) [19,20]. In this context, the importance of the critical shear crack (CSC) kinematics (the opening and sliding of crack lips) to determine the ability of concrete to transfer shear forces has been studied [21–24] based on the CSCT. On the other hand, Marí et al. [25] have proposed a mechanical model that separately considers the most important shear transfer actions.

The expressions used to determine structural elements shear strength in design codes ACI 318-19 [26], Model Code 2010 (Level III Approximation) [27], and CSA A23.3 [28] for beams with shear reinforcement are based on adding a "concrete term" (shear strength provided by concrete, $\boldsymbol{V_c}$) to a "steel term" (shear strength provided by shear reinforcement, $\boldsymbol{V_s}$). The term concrete is attributed to several mechanisms, such as aggregate interlock, dowel action and the shear transmitted across the concrete compression zone. In ACI 318-19, shear strength provided by concrete is based on empirical formulas taken from experimental results, while Model Code 2010 Level III and CSA A23.3 are based on MCFT [7,8], which considers that shear strength provided by concrete reduces with increasing longitudinal reinforcement strains until the strain at yield point. However, Eurocode 2 [29] only consider the stirrups contribution to shear strength, with a variable angle of the compression field. Therefore, only some codes consider a reduction in shear strength with increasing longitudinal reinforcement strain, although they do not contemplate any reduction of shear resistance after the plastic redistribution of internal forces due to the yielding of the flexural reinforcement.

The reduction of the rotation capacity with increasing shear forces for reinforced concrete members without shear reinforcement has been demonstrated by the CSCT [19]. This behaviour has been experimentally verified in shear failures before yielding of the flexural reinforcement [19] and in shear failures after yielding of the flexural reinforcement in statically determined beams [2]. However, there is no experimental evidence of the shear strength reduction with increasing rotation levels in tests conducted on statically indeterminate beams.

The objective of the study presented herein is to analyse the possible influence of the rotation developed by plastic hinges on shear strength in reinforced concrete statically indeterminate beams with shear reinforcement failing in shear after yielding of the flexural reinforcement. For this purpose, an experimental programme has been conducted on statically indeterminate beams failing in shear after yielding of the flexural reinforcement and reaching considerable deformations in the critical plastic regions with an innovative tests system.

2. Experimental programme

2.1. Test specimens

Nine beams (B1 to B9) with 9,000 mm long, 250 mm wide and 450 mm high were tested in 18 different experiments. Each beams was subject to two different shear test types that allowed shear failure to be developed with two different structural typologies: statically determinate structure (hereinafter called *cantilever experiment,* CE) and statically indeterminate structure (hereinafter called *span experiment,* SE).

Each beam was simply supported with cantilevers at both ends and two concentrated loads were applied using two independent hydraulic jacks. The control of these jacks and the different load conditions (load points and test procedure) allowed the two shear test types to be performed.

For the tested specimens, the amount of flexural tensile reinforcement and the slenderness of specimens for both the CE and SE tests were different. The main objective of considering these variables was to allow shear failures to be developed with different rotation levels within a wide range of values, and before or after plastic hinge formation. In this way, it was possible to study how the development of rotations, related to flexural behaviour, governs shear strength in reinforced concrete specimens with shear reinforcement, including those shear failures developed after yielding of the longitudinal reinforcement.

The nine beams were divided into three series according to the arrangement of the twelve 20 mm-diameter bars comprising the longitudinal reinforcement. These arrangements gave the following longitudinal reinforcement ratios ($\boldsymbol{\rho}$): 1.63% (S1), 2.29% (S2) and 1.94% (S3) (**Fig. 2**). The minimum longitudinal reinforcement ratio was arranged to ensure a shear failure before a flexural failure in the SE tests for all the specimens. The effective depth (distance from the extreme compression fibre to the centroid of the longitudinal tensile reinforcement) was 386, 385 and 389 mm, respectively, for the sections of series S1, S2 and S3.

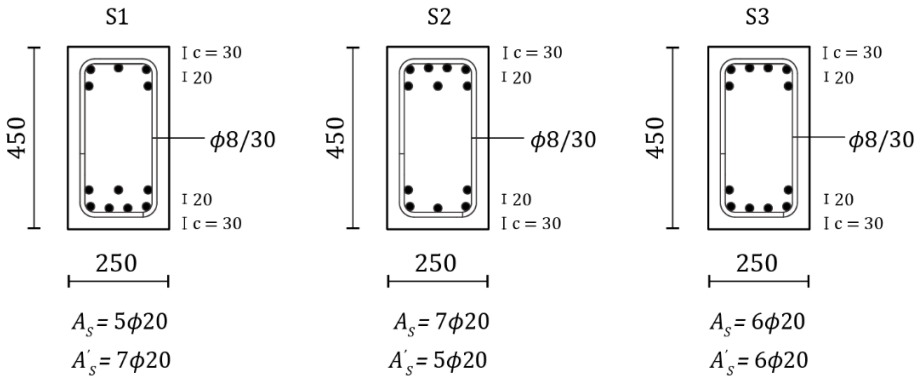

Fig. 2. Reinforcement of series S1, S2 and S3 (dimensions in mm).

The three beams of each series were tested with three different locations for the load and bearing points, both in the CE and SE tests (**Fig. 3**). In the CE tests, the length of the tested cantilevers ($\boldsymbol{l_1}$) was 1,000 mm (L1), 1,620 mm (L1.6), and 2,310 mm (L2.3). In the SE tests, the length of the span ($\boldsymbol{l_2}$) was 6,000 mm (L6), 5,000 mm (L5), and 4,000

mm (L4). In addition, both the length of the cantilever considered (l_3) and the distance between the support A section and the section of applied load P_2 (l_a) were constant and equalled 1,000 mm for all the specimens.

Shear failure was forced to take place in the selected beam regions (l_1 for the CE tests and l_c for the SE tests, according to **Fig. 3**), which were reinforced with two-legged closed stirrups with an 8-mm diameter and a spacing of 30 mm (ϕ8/30, shear reinforcement ratio ρ_w of 0.13%). Outside the expected failure regions, stirrups were provided to prevent shear failure with a reinforcement ratio of 0.90%.

The summary of the reinforcement and geometry of all the specimens is in **Table 1**.

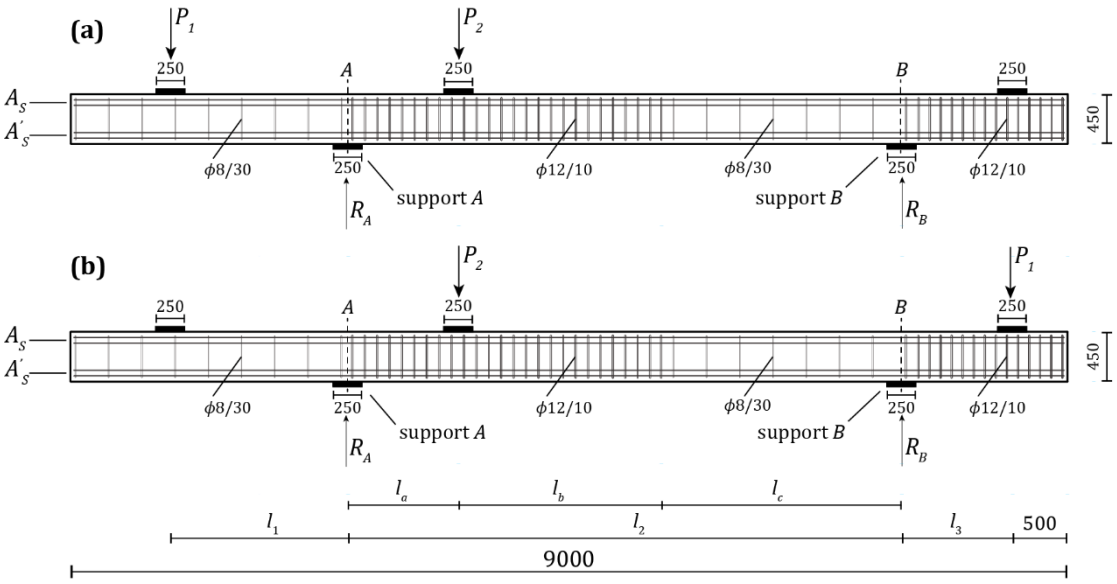

Fig. 3. Geometry of specimens: (a) cantilever experiment (CE); (b) span experiment (SE) (dimensions in mm).

Table 1. Reinforcement and geometry of specimens.

Specimen	A_s	A'_s	ρ (%)	l_1 (mm)	l_2 (mm)	l_b (mm)	l_c(mm)
B1	5ϕ20	7ϕ20	1.63	1000	6000	3100	1900
B2	7ϕ20	5ϕ20	2.29	1000	6000	2500	2500
B3	6ϕ20	6ϕ20	1.94	1000	6000	2800	2200
B4	5ϕ20	7ϕ20	1.63	1620	5000	2100	1900
B5	7ϕ20	5ϕ20	2.29	1620	5000	1500	2500
B6	6ϕ20	6ϕ20	1.94	1620	5000	1800	2200
B7	5ϕ20	7ϕ20	1.63	2310	4000	1100	1900
B8	7ϕ20	5ϕ20	2.29	2310	4000	500	2500
B9	6ϕ20	6ϕ20	1.94	2310	4000	800	2200

A different code with three terms was used to label each test conducted on specimens. The first term denoted the tested beam and the type of test ("C" for the CE test and "S" for the SE test). The second term represented the specimen section according to the flexural reinforcement (S1, S2 or S3). The third term indicated the location of the load and bearing points by indicating the length of the cantilever in the CE tests (L1, L1.6 or L2.3) and the length of the span in the SE tests (L6, L5 or L4). Following this notation, test B1S-S1-L6 was the SE test conducted on the beam B1 (B1S) and the specimen had a flexural reinforcement ratio of 1.63% (S1) and a total length of the span of 6,000 mm (L6).

2.2. Material properties

The compressive strength, modulus of elasticity and tensile strength of concrete, as well as the age of each specimen at the time of testing, are summarised in **Table 2**. The properties of concrete were measured according to UNE-EN 12390 [30–32] and were the average of two tested concrete cylinders (300 mm high, 150 mm diameter). The modulus of elasticity values corresponded to secant stiffness and tensile strength was obtained from the indirect tensile strength tests. The amount of Portland cement in concrete was 325 kg/m^3, the water/cement ratio was 0.52 and the maximum aggregate size was 10 mm.

Table 2. Average values of the concrete properties.

Specimen	Age at testing (days)	f_c(MPa)	E_c (GPa)	f_{ct} (MPa)
B1	33	24.1	24.3	2.5
B2	33	22.3	25.8	3.1
B3	42	22.8	24.4	2.8
B4	57	22.3	24.1	2.6
B5	71	34.7	31.2	3.6
B6	63	35.9	32.8	3.3
B7	88	36.2	34.2	2.9
B8	32	34.5	30.0	3.4
B9	39	29.7	29.4	2.2

The diameter, modulus of elasticity, steel yield stress, steel tensile strength and steel strain values at ultimate strength are summarised in **¡Error! No se encuentra el origen**

de la referencia.. The properties of reinforcement steel were measured according to UNE-EN ISO 6892 [33] and were the average of two tested specimens. The tension tests were load-controlled before yielding at a loading speed of 10 MPa/s, and were displacement-controlled thereafter.

Table 3. Average values of the flexural and transversal reinforcement properties.

Specimens	B1-B3		B4-B9	
ϕ (mm)	8	20	8	20
E_s (GPa)	198	218	183	213
f_y (MPa)	543	557	549	540
f_u (MPa)	677	665	651	649
ε_u (%)	9.6	10.9	11.1	13.5
f_u/f_y	1.25	1.19	1.19	1.20

2.3. Instrumentation

A series of four load cells was used to take continuous measurements of the force in the hydraulic jacks and the reaction at the bearing points. Therefore, redundancy in the force measurements appeared.

Strain gauges of 120 Ω resistance and a 1.5 mm measuring length measured strains in reinforcement steel. There were 58 gauges in each beam glued on the top and bottom longitudinal reinforcements and also on shear reinforcement (**Fig. 4a**).

Displacement transducers with actuating rod potentiometrics up to 150, 200, and 300 mm performed displacement measurements on the concrete surface. A triangulation with 17 transducers (horizontal transducers at the top and bottom flexural reinforcements, vertical transducers at the stirrups location, and diagonal ones) was arranged in each experiment to control deformations in the shear failure zones (**Fig. 4b**). Deflection of specimens was measured on the bottom surface with several displacement transducers (**Fig. 4b**). At the load points, deflection was also measured with the absolute non-contact position sensors integrated into the hydraulic jacks. Two displacement transducers were used to control the slope in the support sections (**Fig. 4b**).

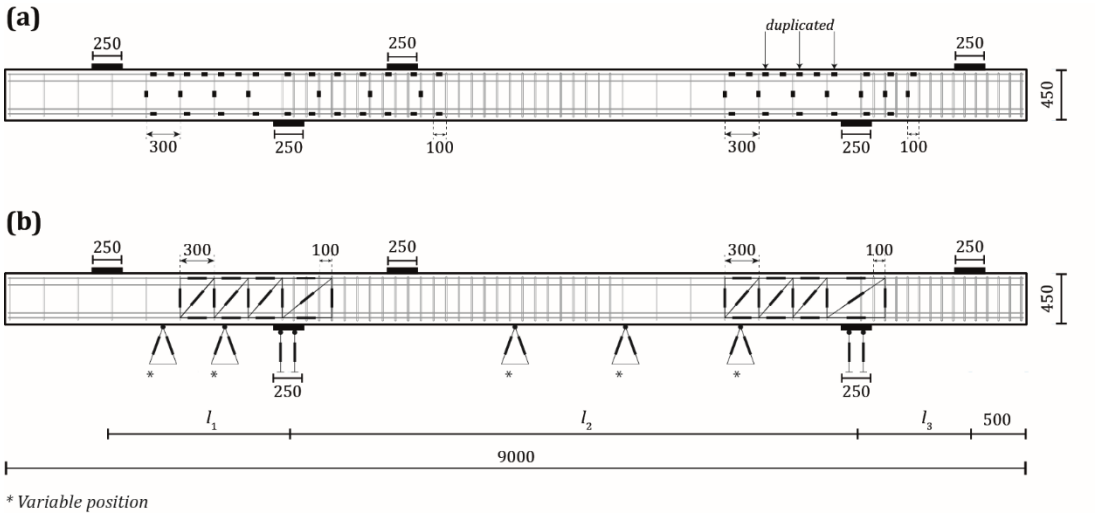

Fig. 4. Instrumentation: (a) strain gauges; (b) displacement transducers (dimensions in mm).

Digital Image Correlation (DIC) was used to obtain accurate measurements of the displacement field of specimens. Photogrammetry was performed on the entire surface of beams with several Canon EOS 5D Mark II digital cameras (21.1 megapixels), equipped with a fixed-focus lens Canon EF 85 mm f/1.8 USM. The image acquisition rate during tests was 2 Hz (up to 3 Hz in several tests). Calibration was done with the Vision Assistant of National Instruments software, and took into account the distortion and projection parameters so that each calibration was valid only for one camera in a specific test. Image calibration was carried out with a dot grid and the obtained resolution was 0.2 mm/pixel. A displacement field was obtained from the images analysis performed with an own software developed using the NI-IMAQ driver and programming with LabVIEW. Each image was divided into a grid of squared facets of 100 x 100 pixels to track displacements between pictures. The software maximum error of the computed displacements was 1/32 pixels.

2.4. Tests system (setup and procedure)

The test setup is illustrated in **Fig. 5.**

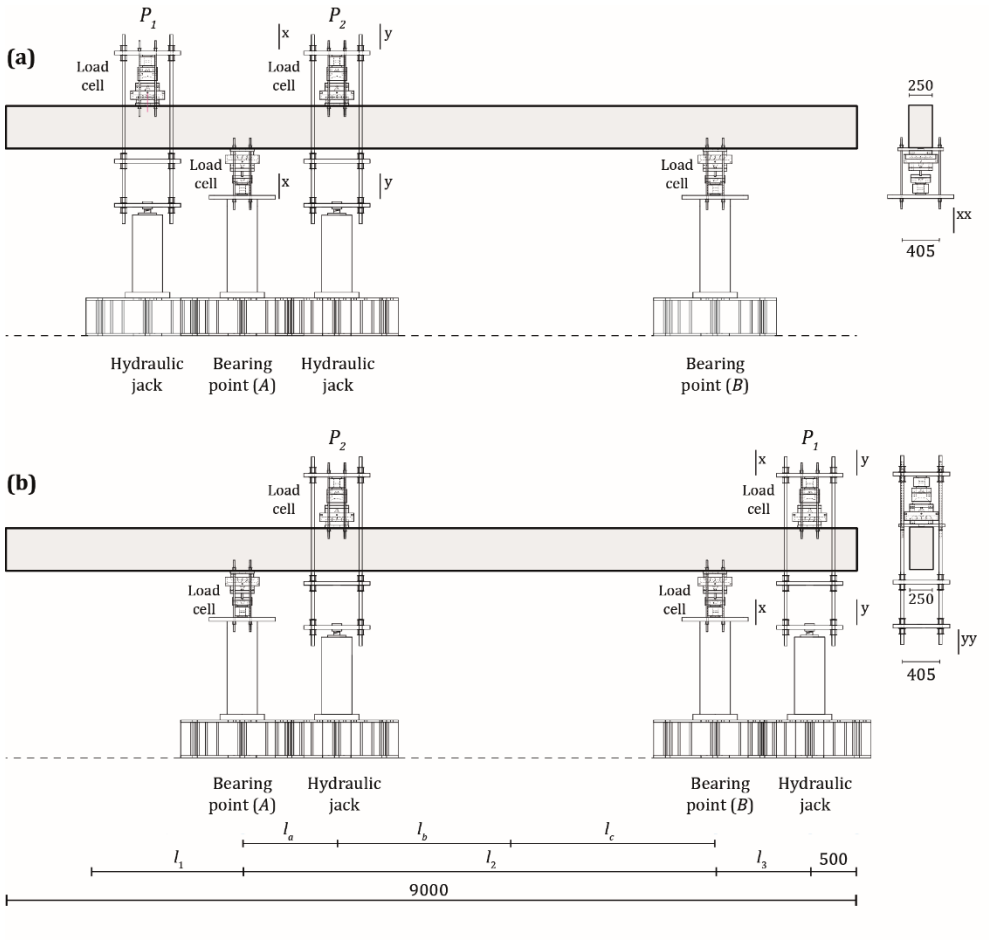

Fig. 5. Test setup: (a) cantilever experiment (CE); (b) span experiment (SE) (dimensions in mm).

Loads and support reactions were transmitted to the beam through steel plates measuring 250 x 250 x 40 mm. Both bearing and load systems allowed horizontal in-plane displacements and rotations. One of the bearing points had a restrained horizontal displacement during tests.

In the CE test, load $\boldsymbol{P_1}$ was applied with displacement control (0.02 mm/s) until the shear failure, and $\boldsymbol{P_2}$ was applied with load control according to the increase in load $\boldsymbol{P_1}$ to obtain no reaction in support $\boldsymbol{B}$ (**Fig. 6a**). As with a statically determinate structure, shear and bending increased simultaneously with a constant shear span until shear failure either before the yielding of the flexural reinforcement or afterwards, which led to a shear failure with constant shear (**Fig. 6b**).

In the SE tests, the performed test procedure allowed shear failures to develop after yielding of the tensile reinforcement over support *B,* as well as the development of considerable rotations.

Each SE test was carried out in two phases (**Fig. 6c**). In the first phase, $\boldsymbol{P_1}$ was applied with displacement control (0.02 mm/s), and $\boldsymbol{P_2}$ with load control, according to the increase in load $\boldsymbol{P_1}$ to obtain no reaction in support $\boldsymbol{A}$. This phase ended when the top longitudinal reinforcement at the support $\boldsymbol{B}$ section yielded and led to a certain slope at the support $\boldsymbol{B}$ section ($\boldsymbol{\theta_{B,I}}$). In addition, at the end of this phase, the shear force along the span was considerably lower than the shear strength of the beam, and the rotation capacity of the plastic hinge at support $\boldsymbol{B}$ section did not develop yet. This enabled a further increase in shear along the span by applying new increments of $\boldsymbol{P_2}$ in the following phase. So, in the second phase, $\boldsymbol{P_2}$ was applied with displacement control (0.02 mm/s), and $\boldsymbol{P_1}$ with load control, according to the increase in load $\boldsymbol{P_2}$ to keep the slope at the support $\boldsymbol{B}$ section blocked. In this phase, this slope was kept constant and equal to that reached at the end of the first phase ($\boldsymbol{\theta_B = \theta_{B,I}}$). This meant that support $\boldsymbol{B}$ behaved as a fixed rotation support, while $\boldsymbol{P_2}$ increased until shear failure.

It was in the second phase of the SE when beams became statically indeterminate structures as moments were given by compatibility conditions because of the restriction imposed for the slope at the support $\boldsymbol{B}$ section ($\boldsymbol{\theta_B = \theta_{B,I}}$). In this phase, shear forces increased with increasing rotations of the plastic hinge thanks to the imposed restriction for the slope at the support $\boldsymbol{B}$ section (branch A in **Fig. 6d**). This restriction was not the equivalent to keeping the load $\boldsymbol{P_1}$ constant in the second phase because, with an imposed $\boldsymbol{P_1}$, the beam would simply have a continuity constant moment imposed at support $\boldsymbol{B}$ section. Under these conditions, increasing load $\boldsymbol{P_2}$ would lead to a decrease of the rotation of the plastic hinge with increasing shear forces (branch B in **Fig. 6d**). Actually, in the tested beams, slight increases in load $\boldsymbol{P_1}$ were necessary to maintain the

slope in this phase ($\boldsymbol{\theta_{B,I}}$) and they were responsible for developing further rotations in the plastic hinge.

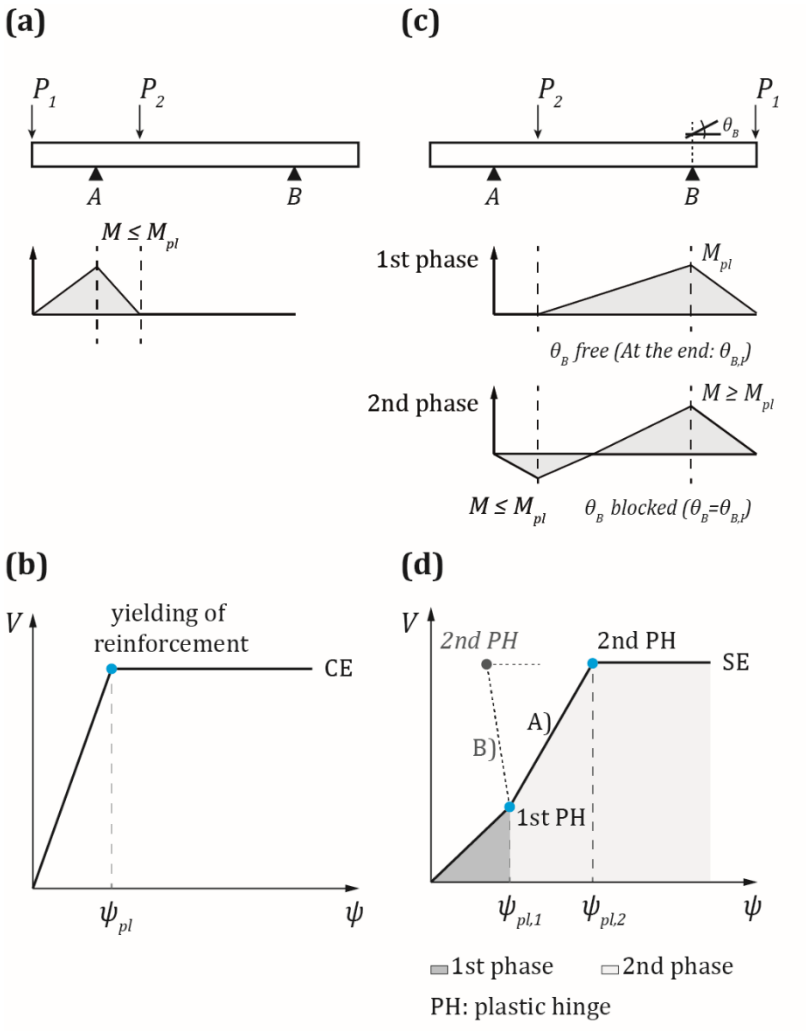

Fig. 6. Tests procedure: (a) cantilever experiment (CE); (b) shear forces and rotation relation in the cantilever experiment (CE); (c) the two phases of the span experiment (SE); (d) the shear forces and rotation relation in the span experiment (SE) for the two different phases.

It is noteworthy that, after yielding of the flexural reinforcement, shear forces were constant (independently of the level of rotation) in the CE tests, whereas the tests system allowed the beam to turn into a statically indeterminate structure in which both rotations and shear forces could simultaneously increase in the SE tests. This makes it easier to obtain a shear-rotation path with shear strength values linked to values of rotation larger than that corresponding to the strain at yield point of the flexural reinforcement.

Finally, and related to the evolution of the SE tests, in the first phase, the shear span between $\boldsymbol{P_2}$ and section *B* was constant, and the shear and bending moment increased simultaneously, as in the CE tests. However, in the second phase, shear span decreased and reached its minimum value at shear failure, and shear increased while the bending moment decreased along the span due to the imposed conditions (**Fig. 6c**).

3. Test results and discussion

3.1. Load-deflection relationship

Fig. 7a and **Fig. 7b** show the load-deflection curves for all the specimens in the CE and SE tests, respectively. For the CE tests (**Fig. 7a**), load $\boldsymbol{P_1}$ is plotted against the deflection under this load ($\boldsymbol{\delta_1}$). For the SE tests (**Fig. 7b**), load $\boldsymbol{P_2}$ is plotted against the deflection under this load ($\boldsymbol{\delta_2}$).

Different load-deflection responses can be observed depending on the type of experiment (CE or SE), the shear slenderness and the arrangement of the longitudinal reinforcement of the specimens.

In the CE tests, load-deflections curves of beams with a brittle shear failure exhibited a sharp drop of load after reaching the maximum load. Otherwise, if the tensile reinforcement yielded before failing in shear, the curves showed a plateau.

In the SE tests, the load-deflection curves showed two (or three in some tests) different branches. The first corresponded to the first test phase; it had a negative slope and the increase in $\boldsymbol{P_2}$ was reduced because the applied load in this phase was $\boldsymbol{P_1}$. The second branch reflected the increase in $\boldsymbol{P_2}$ and the large beam deflection under it in the second phase; that is, after the first plastic hinge developed and before yielding of the bottom reinforcement under this load. On this ascending branch, some beams failed in shear. However, in other cases, shear failure occured on a third plateau-shaped branch, after the development of the second plastic hinge.

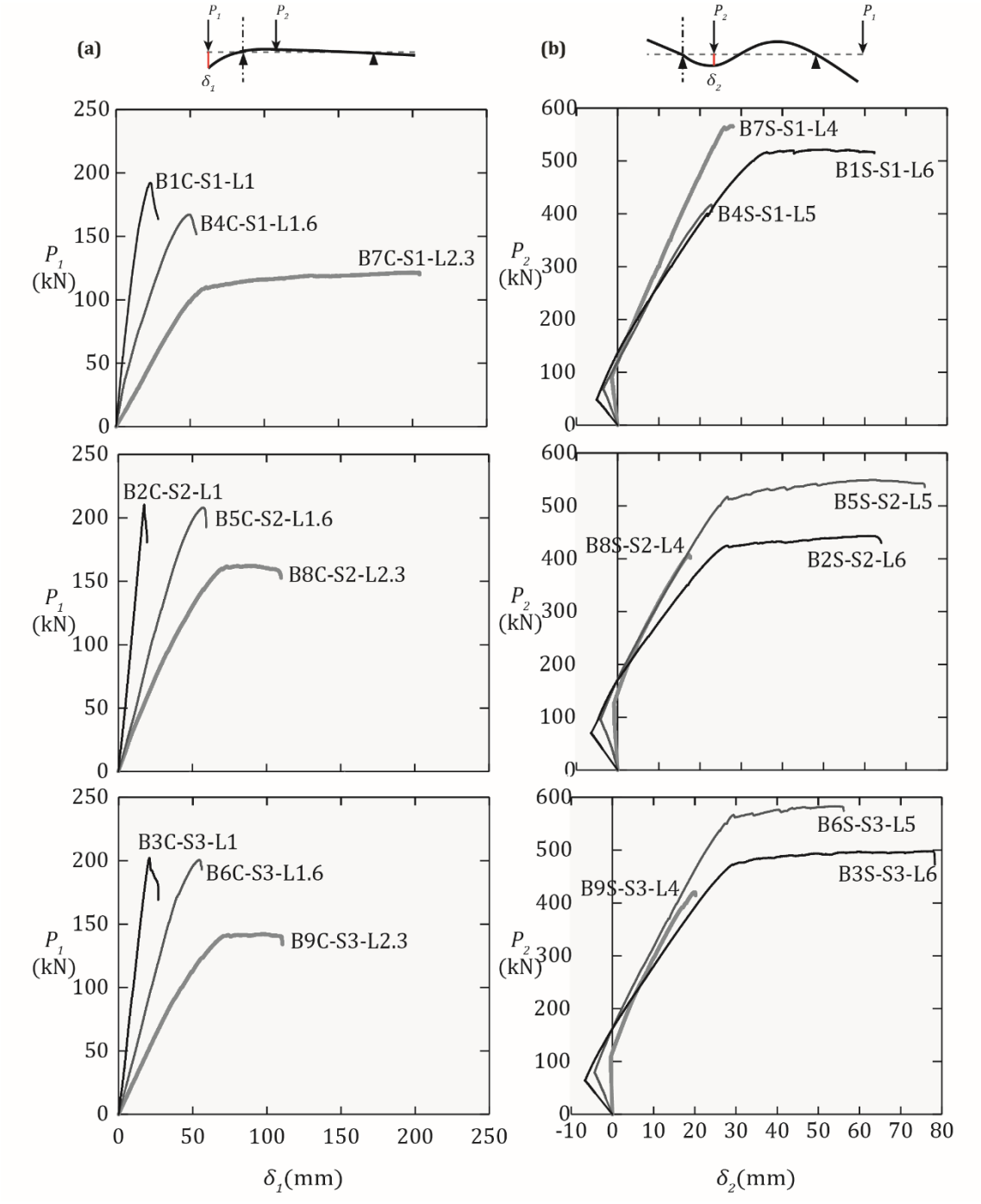

Fig. 7. Load-deflection curves for all the specimens: (a) cantilever experiment (CE); (b) span experiment (SE).

3.2. Shear strength and failure mode

Table 4 summarizes the main results of the tests at failure. It includes the loads applied at failure ($\boldsymbol{P_{1,R}}$ and $\boldsymbol{P_{2,R}}$), as well as the bending moment at failure ($\boldsymbol{M_{1,R}}$) at $\boldsymbol{d/2}$ from the corresponding support (***A*** for CE and ***B*** for SE), and the bending moment at failure ($\boldsymbol{M_{2,R}}$)

at $d/2$ from the section of the applied load P_2 for SE. It is also given the shear strength ($V_{R,test}$) at $d/2$ from the corresponding support (A for CE and B for SE), as well as the equivalent shear span ($a = M_{1,R}/V_{R,test} + d/2$), and the shear slenderness ratio (a/d) at failure for both the cantilever and span experiments. Shear was checked in a control section located at $d/2$ from the applied load according to the CSCT [19], and bending moments and shear strength included self-weight. The shear slenderness ratio (a/d) was constant in the CE tests, but it decreased in the second phase of the SE tests. **Table 4** offers the lowest values obtained at failure in the tests.

Table 4. The main results at failure of the tests for both the cantilever and span experiments.

Sp.	Test	Type	$P_{1,R}$ (kN)	$P_{2,R}$ (kN)	$M_{1,R}$ (mkN)	$M_{2,R}$ (mkN)	$V_{R,test}$ (kN)	a (m)	a/d	ψ_b (mrad)	ψ_s (mrad)	w_{st} (mm)
B1	B1C-S1-L1	V (B)	192.6		155.4		196.2	0.99	2.55	10.6	NA	4.4
B2	B2C-S2-L1	V (B)	210.4		169.6		214.0	0.98	2.56	3.5	NA	2.0
B3	B3C-S3-L1	V (B)	202.1		163.1		205.8	0.99	2.54	8.9	NA	1.7
B4	B4C-S1-L1.6	V (B)	167.2		243.1		173.6	1.59	4.13	11.6	6.3	2.8
B5	B5C-S2-L1.6	V (B)	208.1		300.8		214.5	1.59	4.14	13.1	11.7	2.6
B6	B6C-S3-L1.6	V (B)	200.6		290.3		207.1	1.60	4.14	14.4	5.7	3.5
B7	B7C-S1-L2.3	M	121.5		271.1		-	-	-	-	-	-
B8	B8C-S2-L2.3	V (A)	162.0		356.5		171.3	2.27	5.91	30.7	3.5	1.8
B9	B9C-S3-L2.3	V (A)	142.1		314.5		151.4	2.27	5.84	26.4	1.9	1.9
B1	B1S-S1-L6	V (2 PH)	276.8	521.2	249.4	404.3	148.9	1.87	4.84	36.4	0.8	3.5
B2	B2S-S2-L6	V (2 PH)	373.2	442.8	345.4	316.6	150.7	2.48	6.45	35.3	4.4	0.5
B3	B3S-S3-L6	V (2 PH)	340.0	492.6	311.0	378.0	156.6	2.18	5.61	53.8	5.8	3.4
B4	B4S-S1-L5	V (1 PH)	269.9	415.4	243.6	252.5	143.2	1.89	4.91	25.3	1.7	3.3
B5	B5S-S2-L5	V (2 PH)	381.5	548.8	344.2	345.9	197.3	1.94	5.03	46.2	5.5	2.6
B6	B6S-S3-L5	V (2 PH)	349.5	583.1	313.1	359.9	192.5	1.82	4.68	41.3	1.0	1.4
B7	B7S-S1-L4	V (1 PH)	293.5	562.8	252.7	292.4	214.1	1.37	3.56	15.7	7.7	1.6
B8	B8S-S2-L4	V (1 PH)	382.7	406.1	344.3	170.3	202.4	1.89	4.92	22.6	5.2	1.3
B9	B9S-S3-L4	V (1 PH)	337.6	420.4	301.7	181.4	190.1	1.78	4.58	14.8	12.5	2.5

Note: V (shear failure); M (bending failure); A (after yielding); B (before yielding); PH (plastic hinge); NA (no available data).

All the specimens, except test B7C-S1-L2.3, failed in shear, but with different cracking patterns at failure. However, the differences in the test procedure between the cantilever and span experiments led to differences in the failure mode of specimens.

In the CE tests (statically determinate structure), specimens L1 and L1.6 failed in shear before yielding of the flexural reinforcement (branch A, **Fig. 1**). Specimens of the tests B8C-S2-L2.3 and B9C-S3-L2.3 failed in shear after yielding of the flexural reinforcement (branch B, **Fig. 1**). In these tests, the displacement control of the applied load $\boldsymbol{P_1}$ enabled plastic strains to develop in the flexural reinforcement after reaching the yielding. This led to a shear failure with increasing deformations under constant load. Specimen of the test B7C-S1-L2.3 failed in bending.

In the SE tests (statically indeterminate structure), shear failures developed in the second phase, after the redistribution of internal forces because of the previous yielding of the longitudinal reinforcement and the development of an imposed plastic hinge rotation. Two different behaviours were observed in these SE tests, which depended on the development, or not, of the second plastic hinge under load $\boldsymbol{P_2}$.

As an example of the two different behaviours, **Fig. 8** reflects the evolution of bending moments ($\boldsymbol{M_1}$ and $\boldsymbol{M_2}$) and shear in span ($\boldsymbol{V}$) with the deflection under load $\boldsymbol{P_2}$ for two distinct specimens. In tests B4S-S1-L5, B7S-S1-L4, B8S-S2-L4 and B9S-S3-L4 (test B9S-S3-L4 is plotted in **Fig. 8a**) only one plastic hinge developed and they failed suddenly in shear near the support $\boldsymbol{B}$ section (branch C, **Fig. 1**). In tests B1S-S1-L6, B2S-S2-L6, B5S-S2-L5, B3S-S3-L6 and B6S-S3-L5 (test B3S-S3-L6 is plotted in **Fig. 8b**) developed two plastic hinges before failing in shear (branch D, **Fig. 1**).

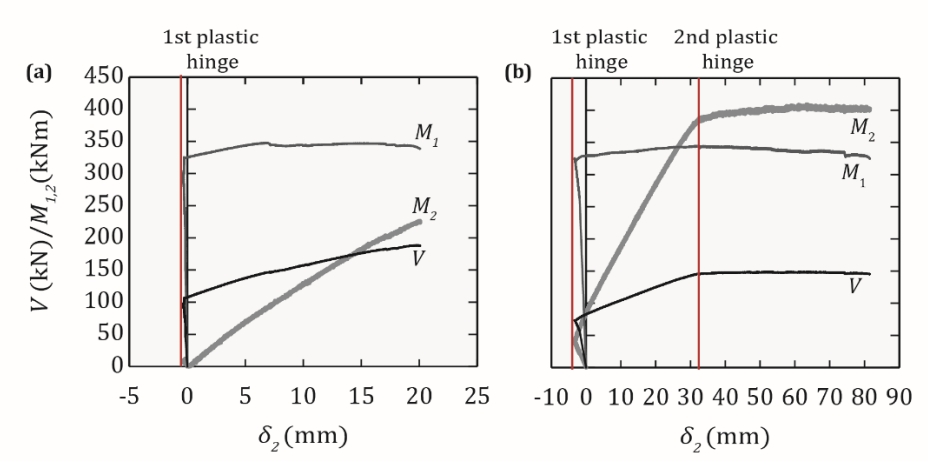

Fig. 8. Evolution of the bending moments (M_1 and M_2) and shear in span (V) *versus* the deflection under load P_2 in the span experiments (SE): (a) test B9S-S3-L4; (b) test B3S-S3-L6.

3.3. Shear strength components

To study the influence of rotation on shear strength in reinforced concrete beams with shear reinforcement, the shear strength was divided into two components: shear strength provided by shear reinforcement ($\boldsymbol{V_s}$) and shear strength provided by concrete ($\boldsymbol{V_c}$), which included the other shear-transfer actions.

The shear strength provided by shear reinforcement ($\boldsymbol{V_s}$) as the sum of the tensile force of all the stirrups ($\boldsymbol{V_{sw}}$) crossed by the CSC was:

$$\boldsymbol{V_s} = \sum \boldsymbol{\sigma_{sw}} \cdot \frac{\boldsymbol{\phi^2 \cdot \pi}}{\boldsymbol{4}} \quad (1)$$

where $\boldsymbol{\phi}$ is the diameter of the bar and $\boldsymbol{\sigma_{sw}}$ is the normal stress for a single stirrup (two branches).

The normal stress for a single stirrup $\boldsymbol{\sigma_{sw}}$ can be calculated by following the procedure of Campana et al. [21] (**Fig. 9a**). At the location where the crack intercepted each considered stirrup, the opening of the crack along the vertical direction ($\boldsymbol{w_i}$) was obtained by DIC. Two points vertically aligned with the stirrup (one on each side of the crack) were considered to obtain this crack opening (**Fig. 9b**). The stress distribution along the stirrup between these two points can be obtained by assuming rigid-plastic bond behaviour [34] for the reinforcement embedded in concrete (**Fig. 9c**). According to this methodology,

bond stress is constant ($\tau_{b1} = 2f_{ct}$) before yielding and the decrease in steel stress is linear with the distance to the crack. After yielding, bond stress reduces ($\tau_{b2} = \tau_{b2}/2$) to consider the decreasing bond stress. The value of f_{ct} is provided in **Table 2**. In addition, a bilinear hardening stress-strain relationship of steel was considered with a tangent modulus of $(f_u - f_y)/(\varepsilon_u - f_y/E_s)$ (**Fig. d**) with the values of the steel properties shown in **¡Error! No se encuentra el origen de la referencia..**

If concrete strains are neglected, w_i must be equal the integration of steel strains:

$$w_i = \int_{l_j+l_k} \varepsilon_{sw} dx \tag{2}$$

This condition allowed the shear strength provided by shear reinforcement ($V_{s,test}$) to be obtained. Due to crack shape, only two stirrups accounted for calculating the shear reinforcement contribution in all cases as those stirrups intercepted by the horizontal branch of the CSC were not considered [21, 35]. Moreover, the considered stirrups were yielded at shear failure in all cases.

The shear strength provided by concrete was calculated as the difference between the total shear strength and that corresponding to shear reinforcement ($V_{c,test} = V_{R,test} - V_{s,test}$). This shear strength ($V_{c,test}$) considered the contribution of different shear-transfer actions, such as aggregate interlock, residual tensile strength, dowelling action or the contribution of the compression chord.

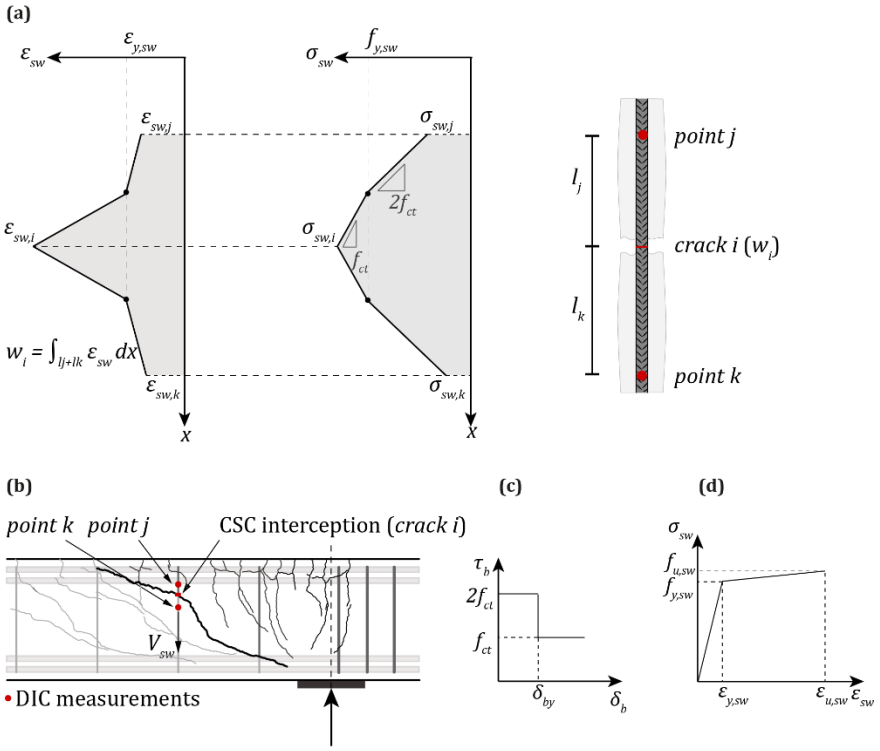

1

Fig. 9. Shear provided by shear reinforcement: (a) relation linking crack opening and steel strain and stresses in the reinforced concrete tie; (b) obtaining the crack opening along the vertical direction by DIC; (c) the considered rigid-plastic bond behaviour; (d) the considered bilinear hardening stress-strain relation of steel (figure developed from Campana et al. [21]).

2 **Fig. 10** shows the contribution of both shear reinforcement and concrete to shear

3 strength. The $\boldsymbol{V_{s,test}/V_{R,test}}$ and $\boldsymbol{V_{c,test}/V_{R,test}}$ ratios are plotted for all the specimens

4 and all the tests: CE (**Fig. 10 a**) and SE (**Fig. 10 b**).

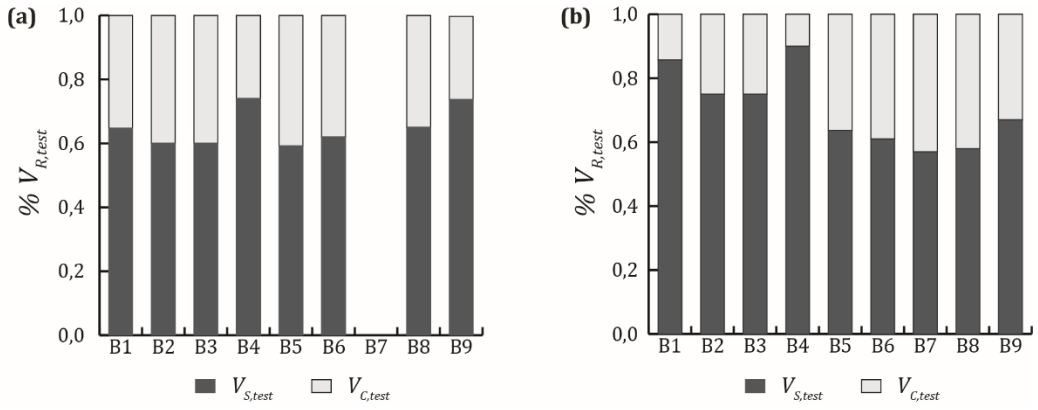

5

Fig. 10. Contribution of shear reinforcement and concrete to shear strength: (a) cantilever experiment (CE); (b) span experiment (SE). (Test B7C-S1-L2.3 not included: bending failure.)

6

3.4. Rotations

Bending rotation ($\boldsymbol{\psi_b}$) was obtained from integrating the bending curvatures along the length of the beam where the CSC developed. In all specimens, the development length of the CSC extended approximately to $\boldsymbol{2d}$ from the support section (*A* for CE and *B* for SE) (**Fig. 11**). In addition, this length covered the development region of the plastic hinge in the SE tests. Bending curvatures were calculated from the longitudinal strains of the top and bottom fibres of the beam, which were measured by DIC. This rotation corresponded to the bending deformation, so it was independent of shear crack evolution. The bending rotation values at failure for all the specimens and tests are summarised in **Table 4**.

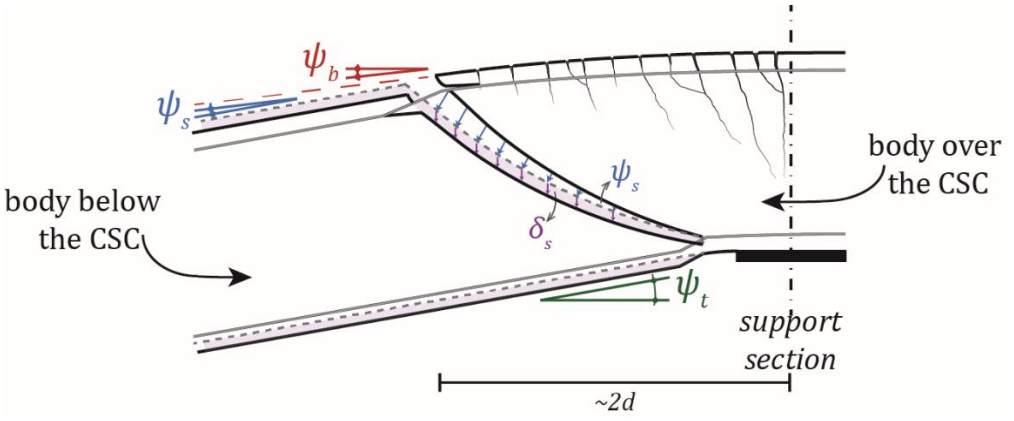

Fig. 11. Kinematics of the critical shear crack and definition of bending, total and crack rotation along its development length.

The CSC divided the beam into two different bodies, one located over the CSC and the other located below it. The body over the CSC only developed the bending rotation ($\boldsymbol{\psi_b}$), as previously explained, but the body below also underwent an extra rotation caused by the development of the CSC. As a result, the total rotation of the body below, measured by DIC, was larger than the bending one. This total rotation ($\boldsymbol{\psi_t}$) was obtained as the difference between the slope of the bottom fibres at a support section (*A* for CE and *B* for SE) and the maximum slope at the end of the development length of the CSC (**Fig. 11**). It must be pointed out that the slope of the support section in the second phase of

the SE tests was constant due to the block of the support (the DIC measurements reflected this condition).

The extra rotation obtained as the difference between the measured rotation of the body below (ψ_t) and over (ψ_b) the CSC was assumed the crack rotation ($\psi_s = \psi_t - \psi_b$). This rotation was linked to the evolution of the CSC, so it was directly related to shear deformation. For that reason, the crack rotation (ψ_s) may be explained by the CSC kinematics shown in **Fig. 11**. This kinematics can be considered to be governed mainly by a rotational movement (the named crack rotation, ψ_s) with the centre of rotations located near the tip of the crack [21,22,35]. However, as the CSCT points out in recent articles about punching shear failures [24,36], a vertical displacement (δ_s) also related to shear deformation may develop along the CSC. This displacement may be constant or not along the CSC; if it is, the vertical movement does not contribute to increase the slope of the body below the CSC and, consequently, it was not registered by the total rotation (ψ_t) measured at the bottom fibres. The crack rotation values at failure for all the specimens and tests are summarised in **Table 4** (the data for specimens V1 in the CE tests are not available).

The bending (ψ_b) and total rotation (ψ_t) evolution for all specimens in the SE tests *versus* shear force ($V/V_{R,test}$) is plotted in **Fig. 12**. The evolution of these rotations differed throughout the tests. With low shear force levels, both rotations were similar ($\psi_b \sim \psi_t$) because the CSC was not yet developed. However, when shear force increased and caused the development of the CSC, the crack rotation (ψ_s) started and the total rotation increased more than the bending one. The largest difference between the total rotation and the bending one ($\psi_t > \psi_b$) occured in the second phase of the tests because the CSC width increased and led to major crack rotation (ψ_s).

The increase in the CSC width was also related to the amount of shear provided by stirrups. At the points where the CSC crossed the different stirrups, the more the CSC width, the greater stirrup stresses became. Therefore, the shear reinforcement

contribution to shear strength increased with the development of the CSC. This is illustrated by the evolution of the shear strength provided by stirrups ($\boldsymbol{V_s/V_{R,test}}$) for specimens S2 in the SE tests plotted in **Fig. 13a**. Activation of stirrups occurred mainly in the second phase of the SE tests, when crack rotation ($\boldsymbol{\psi_s}$) increased because of the larger crack width (**Fig. 12**). For lower shear slenderness beams, the value of the shear effort along the span increased sooner while the SE test was underway and, as a result, the activation of stirrups occurred earlier (**Fig. 13a**). For the beam with the most slenderness, test B2S-S2-L6, stirrups did not provide shear strength until the first plastic hinge developed, whereas for the beam with the least slenderness, test B8S-S2-L4, stirrups were considerably activated at the same moment of the test. The specimen images of the test B5S-S2-L5 (**Fig. 13b**) illustrate the development of cracks in the second phase of the test.

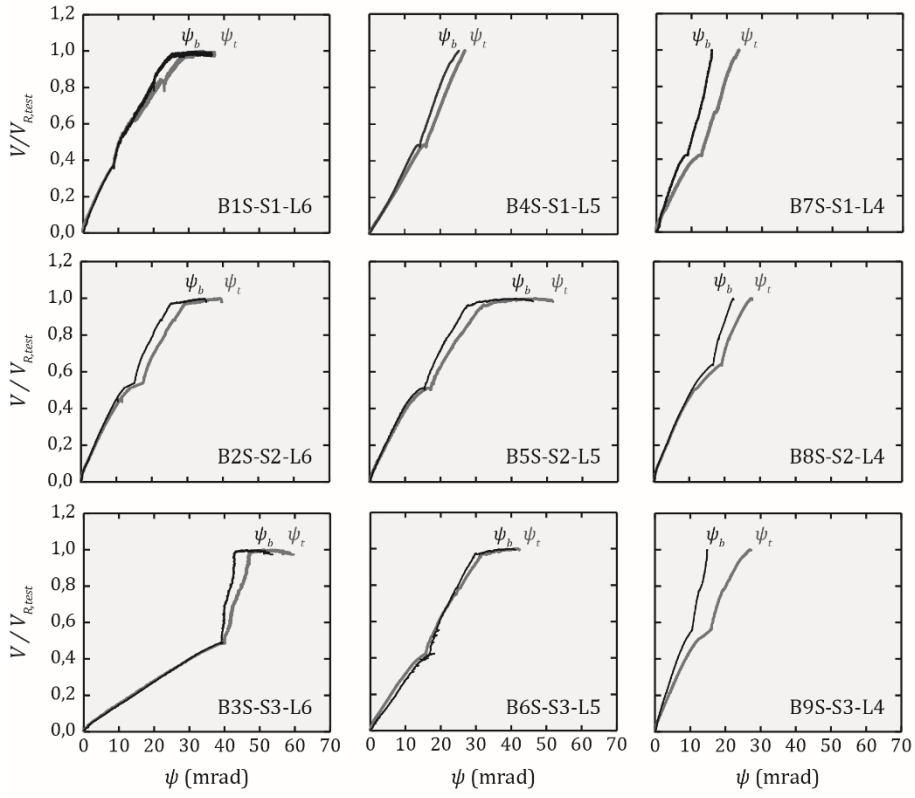

Fig.12. Evolution of the bending and total rotation *versus* shear force for all the specimens in the span experiments (SE).

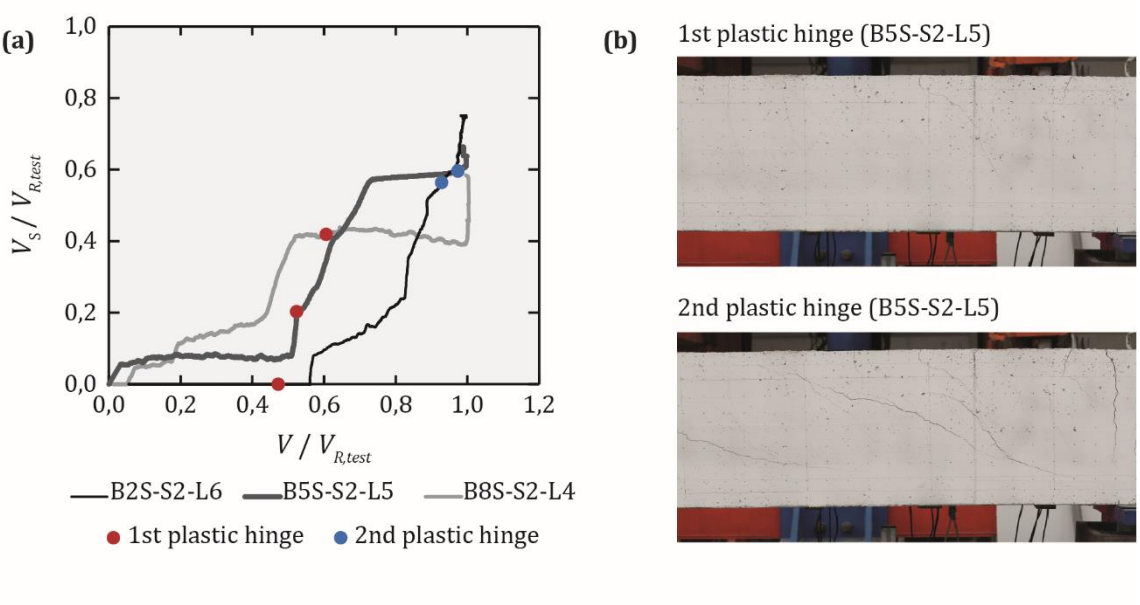

Fig. 13. (a) Evolution of shear strength provided by shear reinforcement *versus* the total shear strength for specimens S2 in the span experiments (SE); (b) specimen images of the test B5S-S2-L5 in the second phase of the span experiment (SE).

3.5. Influence of rotation on the shear strength provided by concrete

The normalised shear strength provided by concrete is plotted *versus* the bending rotation (ψ_b) for all the specimens failed in shear in **Fig. 14**. Shear strength must be normalised according to the compressive strength of concrete to compare different beams. For this normalisation, only the shear strength provided by concrete ($V_{c,test}$) can be considered.

According to **Fig. 14**, the development of larger bending rotations (ψ_b) entailed a decrease in shear strength provided by concrete for the tested reinforced concrete beams with shear reinforcement. This loss of shear strength after yielding of the flexural reinforcement had already been confirmed by tests carried out on statically determinate reinforced concrete beams without shear reinforcement [2]. However, this experimental study extended the analysis to statically indeterminate beams with shear reinforcement and was capable of obtaining shear failures with considerable plastic hinge rotations.

This behaviour agreed with the failure criterion proposed by Vaz Rodrigues et al. [2] that considered the rotation capacity at failure for concrete beams without shear

reinforcement developing plastic strains (the failure criterion plotted in **Fig. 14**). This criterion was based on the CSCT hypothesis [19] and it established a relationship between the shear strength of concrete and beam rotation at failure.

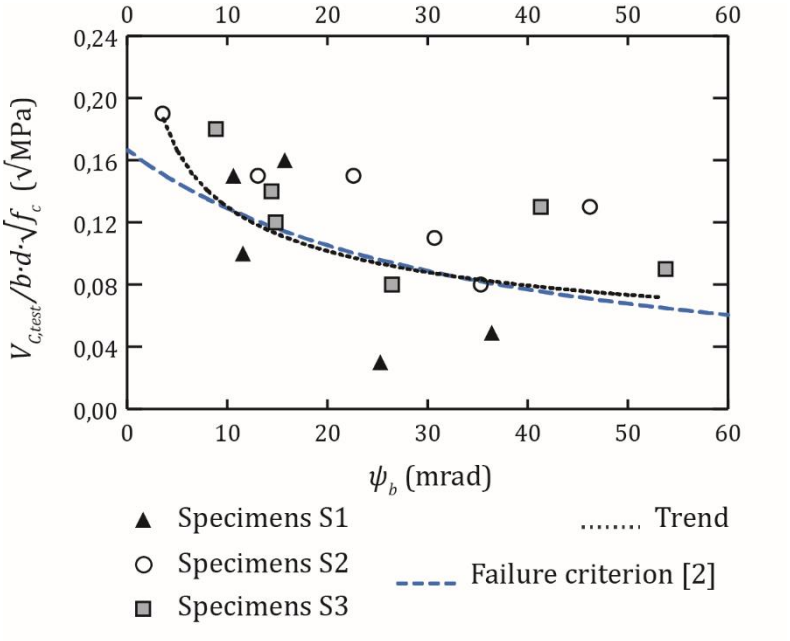

Fig. 14. Shear strength provided by concrete according to bending rotation. (Test B7C-S1-L2.3 not included: bending failure.)

The loss of shear strength provided by concrete for increasing bending rotation may be related to the increase in CSC width as it would entail the reduction of some shear-carrying mechanisms such as aggregate interlock [2,19,20]. This is illustrated in **Fig. 15**, where the normalised shear strength provided by concrete is plotted *versus* the average value of the critical shear crack opening measured in the stirrups section ($\boldsymbol{w_{st}}$) for all the specimens failed in shear. This average value is obtained from the CSC opening measurements performed with DIC in the stirrups section where the crack intercepts each one and in the same directions as them. These average crack width values at failure for all the specimens and tests are summarised in **Table 4**.

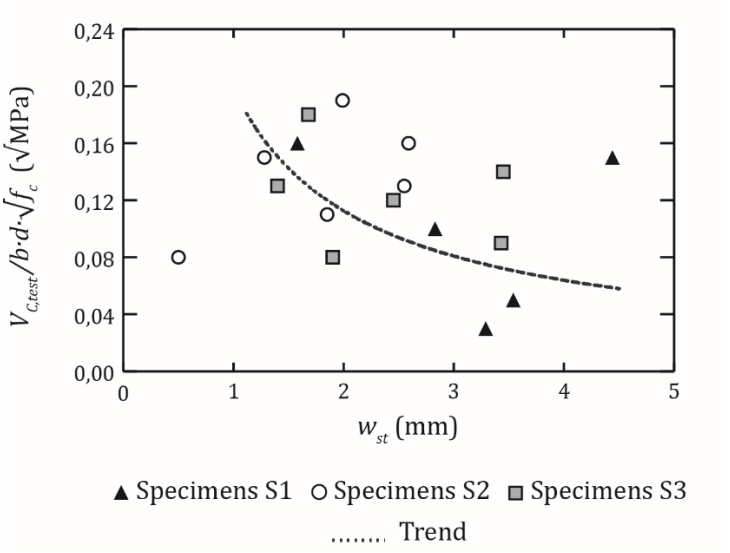

Fig. 15. Shear strength provided by concrete according to the average value of the critical shear crack opening measured in the stirrups section. (Test B7C-S1-L2.3 not included: bending failure.) (Data for specimens L1 of the CE tests is not available.)

4. Comparison of the test results with existing code provisions

In **¡Error! No se encuentra el origen de la referencia.**, the test results are compared with the predicted shear strength of design codes according to the experimented-to-predicted shear strength ratio ($\boldsymbol{V_{R,test}\,/\,V_{Rd}}$). The considered codes are ACI Building Code 318-19 [26] (**Fig. 16a**), Eurocode 2 [29] (**Fig. 16b**), Model Code 2010 (Level I Approximation) [27] (**Fig. 16c**), and Model Code 2010 (Level III Approximation) [27] (**Fig. 16d**). In all cases, $\boldsymbol{\gamma_c}$ = 1.0 and shear strength were optimised by considering the minimum possible angle between web compression and the axis of the member ($\boldsymbol{\theta}$).

In a general approach, the comparison of the experimented-to-predicted shear strength ratio for the different codes of practice with simple formulations (ACI 318-19, Eurocode 2, and MC2010 Level I) shows similar scatter results (**Fig. 16a**, **Fig. 16b** and **Fig. 16c**, respectively). However, whereas ACI 318-19 and Eurocode 2 provide similar mean values of this ratio as well, the shear strength values predicted by MC2010 Level I are very conservative ($\boldsymbol{V_{R,test}/V_{Rd}}$ mean value of 1.66). These “too safe” predictions may be the result of the non-optimised angle $\boldsymbol{\theta}$**,** which is fixed constant in the formulation of Level I. Finally, it is noteworthy that the comparable predictions obtained from ACI 318-19 and

Eurocode 2 are based on very different formulation as the former considers the shear strength provided by both concrete and shear reinforcement, but the latter contemplates only the shear strength provided by steel.

Predictions provided by Level I of the MC2010 can be improved with the Level III formulation (**Fig. 16d**), which is based on the MCFT [7, 8]. This iterative formulation considerably reduces the too conservative predictions of shear strength obtained with Level I and, in addition, provides the least scatter results among the different codes ($\boldsymbol{V_{R,test}/V_{Rd}}$ COV value of 0.09).

Regarding the reduction of shear strength with increasing bending rotation, codes present major differences. The formulation provided by ACI 318-19, Eurocode 2 and MC2010 Level I does not consider this dependence between both values (the trend plotted in **Fig. 16a**, **Fig. 16b** and **Fig. 16c**, respectively). Although MC2010 Level III does not directly consider the bending rotation to be an influential factor, it considers longitudinal reinforcement strains (the trend plotted in **Fig. 16d**). This factor is related to the bending rotation and, as a result, it predicts that shear strength values are dependent on bending deformation. However, this influence is not captured for those strains beyond yielding of the reinforcement because they are calculated from a section analysis by assuming a linear elastic stress-strain relation.

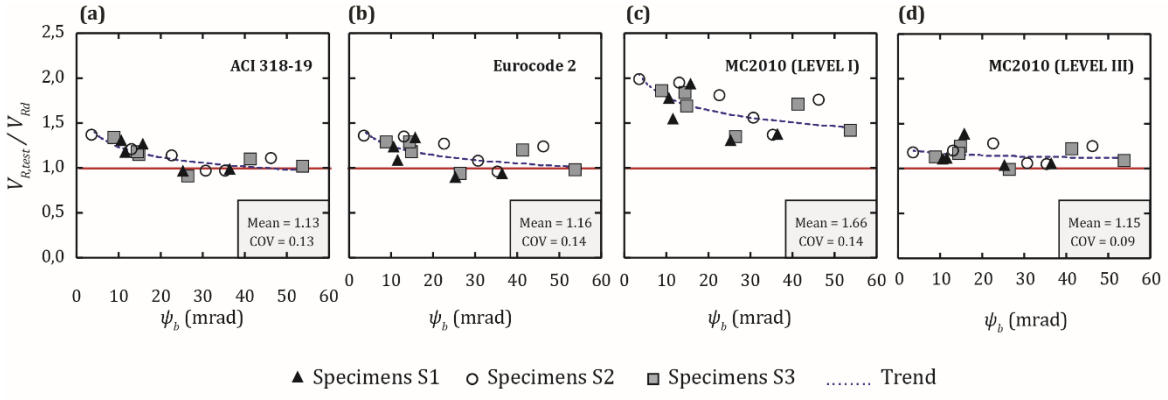

Fig. 16. Comparison made between test results and predicted shear strength calculated according to design codes: (a) ACI Building Code 318-19; (b) Eurocode 2; (c) Model Code 2010 Level I; (d) Model Code 2010 Level III. (Test B7C-S1-L2.3 not included: bending failure.)

5. Conclusions

The influence of the plastic hinge rotation on shear strength in reinforced concrete statically indeterminate beams with shear reinforcement is herein investigated. For this goal, an experimental programme based on an innovative tests system was designed and carried out. The results of 18 shear tests are presented and analysed. The main conclusions are the following:

1. The designed tests system allows statically determinate and indeterminate structures to fail in shear, which entails beams failing in shear before and after yielding of the flexural reinforcement. Tests on statically indeterminate structures allow continuous beams behaviour to be simulated, which results in a plastic redistribution of flexural forces and in large flexural reinforcement strains. The main difference in these tests with shear tests on statically determinate structures is that it is possible to develop shear failures after yielding of the flexural reinforcement with growing shear forces and plastic hinge rotations.
2. The average width of the critical shear crack is obtained with Digital Image Correlation (DIC) technique by the displacement measurements performed at stirrups sections where the crack intercepts them. The shear strength provided by shear reinforcement is calculated from these measurements. The shear

strength provided by the remaining shear resistance mechanisms (shear strength provided by concrete) is calculated by subtracting the shear strength provided by the shear reinforcement from the shear strength recorded in the tests.

3. Rotations throughout the length of the beam where the critical shear crack develops are calculated from displacement measurements performed with DIC. The crack rotation is assumed the difference between the measured rotation of the body below and over the CSC. The first is obtained at bottom fibres of the beam, whereas the second is the bending rotation. The crack rotation is linked to the evolution of the CSC, so it is directly related to shear deformation.

4. As expected, the shear strength provided by concrete decreases as bending rotation increases in reinforced concrete beams with shear reinforcement. After yielding of the flexural reinforcement, the plastic hinge rotation reduces the shear strength capacity because of the loss of shear strength provided by concrete. This behaviour agrees with the failure criterion proposed by Vaz Rodrigues et al. (2) for concrete beams without shear reinforcement developing plastic strains that account for rotation capacity at failure.

5. The shear strength provided by concrete reduces for increasing average widths of the critical shear crack in the tested specimens.

6. Simple formulation from ACI 318-19, Eurocode 2, and MC2010 Level I provide similar scatter results for the ratio of experimented-to-predicted shear strength, although MC2010 Level I predicts very conservative shear strength values. However, the iterative formulation based on the MCFT from the MC2010 Level III considerably reduce these too safe predictions from Level I and give the least scatter results among the different codes. Codes do not properly capture the reduction of shear strength for increasing bending rotations. Only the formulation proposed by MC2010 Level III accounts for the longitudinal reinforcement strains

as an influencing shear strength factor, which is related to the bending rotation, but it is limited to the strain at yield point.

Acknowledgements

This research was funded with grants from the Spanish Ministry of Economy and Competitiveness to Research Project BIA2015-64672-C4-4-R. The experimental programme was developed in the Laboratory of Concrete of the Institute of Concrete Science and Technology (ICITECH) of the Universitat Politècnica de València (UPV), with concrete supplied by Caplansa. Andrea Monserrat was supported by the Conselleria d'Educació, Investigació, Cultura i Esport of the Generalitat Valenciana (Order 6/2015, DOCV no. 7615 15.09.2015) with European Regional Development Funds (ERDF) allocated by the EU.

References

[1] S. M. Lopes and R. N. F. do Carmo, "Deformable strut and tie model for the calculation of the plastic rotation capacity", Comput. Struct., vol. 84, no. 31–32, pp. 2174–2183, 2006.

[2] R. Vaz Rodrigues, A. Muttoni, and M. Fernández Ruiz, "Influence of shear on rotation capacity of reinforced concrete members without shear reinforcement", ACI Struct. J., vol. 107, no. 5, pp. 516–525, 2010.

[3] J. Schlaich, K. Shafer, and M. Jennewein, "Toward a consistent design of structural concrete", PCI J., vol. 32, pp. 74–150, Jan. 1987.

[4] W. Ritter, "Die Bauweise Hennebique (The Hennebique system)", Schweizerische Bauzeitung, vol. Bd. XXXIII, no. 7, 1899.

[5] E. Mörsch, "Der Eisenbetonbau (Concrete-steel construction)", New York: McGraw-Hill, 1909.

[6] A. Muttoni, J. Schwartz, and B. Thürlimann, "Design of Concrete Structures with Stress Fields", Birkhaüser/Springer, 1997.

[7] F. J. Vecchio and M. P. Collins, "The Modified Compression-Field Theory for reinforced concrete elements subjected to shear", J. Proc., vol. 83, no. 2, pp. 219–231, 1986.

[8] F. J. Vecchio, "Disturbed stress field model for reinforced concrete: formulation", J. Struct. Eng., vol. 126, no. 9, pp. 1070–1077, Jan. 2000.

[9] F. Leonhardt, "Reducing the shear reinforcement in reinforced concrete beams and slabs", Mag. Concr. Res., vol. 17, no. 53, pp. 187–198, 1965.

[10] F. Leonhardt, “Shear and torsion in prestressed concrete”, in VI Congress of the Fédération International de la Précontrainte, 1970, pp. 137–155.

[11] Z. P. Bažant and P. G. Gambarova, “Rough cracks in reinforced concrete”, J. Struct. Div., vol. 106, no. 4, pp. 819–842, 1980.

[12] P. G. Gambarova, “On aggregate interlock mechanism in reinforced concrete plates with extensive cracking”, in IABSE Colloquium Delft on “Advanced mechanics of reinforced concrete”, 1981, pp. 99–120.

[13] J. C. Walraven, “Fundamental analysis of aggregate interlock”, ASCE J. Struct. Div., vol. 107, no. 11, pp. 2245–2270, 1981.

[14] J. C. Walraven and H. W. Reinhardt, “Theory and experiments on the mechanical behaviour of cracks in plain and reinforced concrete subjected to shear loading”, Heron, TU Delft, vol. 26, no. 1A, p. 68, 1981.

[15] R. Guidotti, “Poinçonnement des planchers-dalles avec colonnes superposées fortement sollicitées”, École Polytechnique Fédérale de Lausanne, Lausanne, Switzerland, 2010.

[16] S. Dei Poli, P. G. Gambarova, and C. Karakoç, “Aggregate interlock role in RC thin-webbed beams in shear”, J. Struct. Eng., vol. 113, no. 1, pp. 1–19, 1987.

[17] S. Dei Poli, M. Di Prisco, and P. G. Gambarova, “Stress field in web of RC thin-webbed beams failing in shear”, J. Struct. Eng., vol. 116, no. 9, pp. 2496–2515, 1990.

[18] J. A. Ramirez and J. E. Breen, “Evaluation of a modified truss-model approach for beams in shear”, Struct. J., vol. 88, no. 5, pp. 562–572, 1991.

[19] A. Muttoni and M. Fernández Ruiz, “Shear strength of members without transverse reinforcement as function of critical shear crack width”, ACI Struct. J., vol. 105, no. 2, pp. 163–172, 2008.

[20] A. Muttoni, “Punching shear strength of reinforced concrete slabs without transverse reinforcement”, ACI Struct. J., vol. 105, no. 4, pp. 440–450, 2008.

[21] S. Campana, M. Fernández Ruiz, A. Anastasi, and A. Muttoni, “Analysis of shear-transfer actions on one-way RC members based on measured cracking pattern and failure kinematics”, Mag. Concr. Res., pp. 386–404, 2013.

[22] M. Fernández Ruiz, A. Muttoni, and J. Sagaseta, “Shear strength of concrete members without transverse reinforcement: A mechanical approach to consistently account for size and strain effects”, Eng. Struct., vol. 99, pp. 360–372, Sep. 2015.

[23] F. Cavagnis, M. Fernández Ruiz, and A. Muttoni, “An analysis of the shear-transfer actions in reinforced concrete members without transverse reinforcement based on refined experimental measurements”, Struct. Concr., vol. 19, no. 1, pp. 49–64, Feb. 2018.

[24] A. Muttoni, M. Fernández Ruiz, and J. T. Simões, “The theoretical principles of the critical shear crack theory for punching shear failures and derivation of consistent closed-form design expressions”, Struct. Concr., vol. 19, no. 1, pp. 174–190, Feb. 2018.

[25] A. Marí, A. Cladera, J. Bairán, E. Oller, and C. Ribas, “Shear-flexural strength mechanical model for the design and assessment of reinforced concrete beams subjected to point or distributed loads”, Front. Struct. Civ. Eng., vol. 8, no. 4, pp. 337–353, Dec. 2014.

[26] ACI Committee 318, “Building code requirements for structural concrete (ACI 318-19); and commentary (ACI 318R-19)”, American Concrete Institute, Farmington Hills, 2019.

[27] Fédération International du Béton (fib), “Model Code 2010”, Ernst & Sohn, 2012.

[28] CSA Committee A23.3, “Design of concrete structures”, Canadian Standards Association, 2014.

[29] CEN, EN 1992-1-1:2004, “Eurocode 2: Design of concrete structures - Part 1-1: General rules and rules for buildings”, 2004.

[30] UNE EN-12390-3:2009, “Ensayos de hormigón endurecido. Parte 3: Determinación de la resistencia a compresión del hormigón endurecido”, 2009.

[31] UNE EN-12390-6:2010, “Ensayos de hormigón endurecido. Parte 6: Resistencia a tracción indirecta de probetas”, 2010.

[32] UNE EN-12390-13:2014, “Ensayos de hormigón endurecido. Parte 13: Determinación del módulo secante de elasticidad en compresión”, 2014.

[33] UNE-EN ISO 6892-1:2017, “Materiales metálicos. Ensayo de tracción. Parte 1: Ensayo a temperatura ambiente”, 2017.

[34] V. Sigrist, “Zum Verformungsvermögen von Stahlbetonträgern (Deformation capacity of reinforced concrete beams)”, ETH Zürich, 1995.

[35] P. Huber, T. Huber, and J. Kollegger, “Investigation of the shear behavior of RC beams on the basis of measured crack kinematics”, Eng. Struct., vol. 113, pp. 41–58, Apr. 2016.

[36] J. T. Simões, M. Fernández Ruiz, and A. Muttoni, “Validation of the Critical Shear Crack Theory for punching of slabs without transverse reinforcement by means of a refined mechanical model”, Struct. Concr., vol. 19, no. 1, pp. 191–216, Feb. 2018.